IMPLEMENTING MULTI-SCALE AGRICULTURAL INDICATORS EXPLOITING SENTINELS

VEGETATION FIELD DATA AND PRODUCTION OF GROUND-BASED MAPS

"MARAGUA SITE (UPPER TANA BASIN), KENYA"
8TH MARCH, 2016

ISSUE I1.00

EC Proposal Reference N° FP7-311766

Actual submission date : May 2016

Start date of project: 01.11.2012 Duration : 40 months

Name of lead partner for this deliverable: EOLAB

Book Captain: Fernando Camacho (EOLAB)

Contributing Authors: Consuelo Latorre (EOLAB)

Justine Cordingley, Deborah Bossio, Kennedy Waweru Nganga, Janen Gicheha (CIAT)

Project co-funded by the European Commission within the Seventh Framework Program (2007-2013)		
Dissemination Level		
PU	Public	**X**
PP	Restricted to other programme participants (including the Commission Services)	
RE	Restricted to a group specified by the consortium (including the Commission Services)	
CO	Confidential, only for members of the consortium (including the Commission Services)	

DOCUMENT RELEASE SHEET

Book Captain:	F. Camacho	Date: 15.05.2016	Sign. 
Approval:	R. Lacaze	Date:10.06.2016	Sign. 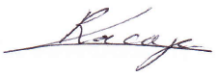
Endorsement:	M. Koleva	Date:	Sign.
Distribution:	Public		

CHANGE RECORD

Issue/Revision	Date	Page(s)	Description of Change	Release
	15.05.2016	All	First Issue	I1.00

TABLE OF CONTENTS

1. Background of the Document 11

1.1. Executive Summary 11

1.2. Portfolio 11

1.3. Scope and Objectives 12

1.4. Content of the Document 12

2. Introduction 13

3. Study area 15

3.1. Location 15

3.2. Description of The Test Site 15

4. Ground measurements 17

4.1. Material and Methods 17

4.1.1 Digital Hemispheric Photographs (DHP) 17

4.2. Spatial Sampling Scheme 20

4.3. Ground data 21

4.3.1. Data processing 21

4.3.2. Content of the Ground Dataset 24

5. Evaluation of the sampling 27

5.1. Principles 27

5.2. Evaluation Based On NDVI Values 27

5.3. Evaluation Based On Convex Hull: Product Quality Flag. 28

6. Production of ground-based maps 30

6.1. Imagery 30

6.2. The Transfer Function 30

6.2.1. The regression method 30

6.2.2. Band combination 31

6.2.3. The selected Transfer Function 32

6.3. The High Resolution Ground Based Maps 33

6.3.1. Mean Values 36

7. Conclusions 38

8. Acknowledgements 39

9. References 40

LIST OF FIGURES

Figure 1: Team involved in the field campaign in Maragua Upper Tana site, Kenya (2016), along with local farmers (those wearing white dressing on the head) in front of a Tee plantation 14
Figure 2: Location of Maragua_Upper Tana site in Kenya. False color composition (RGB – SWIR-NIR-RED) of TOA Reflectance Landsat-8 images over the study area 20 km^2. (Maragua Upper Tana, 8th March, 2016). 15
Figure 3: Landscape views of Maragua site, Kenya, 8th March 2016. 16
Figure 4: Pictures taken during the field campaign (8th March 2016) in Maragua_Upper Tana site (Kenya) over typical fields. 16
Figure 5: Location of the Elementary Sampling Units (ESU) over the study area in Maragua_Upper Tana site. Field campaign (8th-9th March 2016). DHP sampling over Google Earth and TOA Lansdsat-8 footprint. 20
Figure 6: Digital Hemispherical Photographs acquired in Maragua_Upper Tana site (Kenya) during the field campaign on 8-9th March, 2016. Top: Upward Looking. Bottom: Downward Looking. 21
Figure 7: Results of the CAN-EYE processing carried out on ESU 23 (grassland) during the field campaign (8-9th March, 2016). (a) DHP images. (b) Classified images. (c) Average bidirectional gap fraction and (d) the clumping factor versus view zenith angle. 21
Figure 8: Inter-comparison of the calculated biophysical variables LAIeff (left side) and LAI (right side) over the ESUs with different methods: CEV5.1, CEV6.1 and Miller´s formula. Maragua_Upper Tana site (Kenya) during the campaign of 8-9th March, 2016. 22
Figure 9: Examples of understory and overstory over Eucalyptus plantation: ESU 7 (left side) and ESU 11(right side). 23
Figure 10: Inter-comparison of the measured biophysical variables over the ESUs. LAI versus FAPAR, Maragua_Upper Tana site (Kenya). Field campaign (8-9th March). LAI (purple dots) and LAIeff (green dots). 23
Figure 11: Inter-comparison of the measured biophysical variables over the ESUs. FAPAR versus FCOVER, Maragua Upper Tana site (Kenya). Field campaign (8th March, 2016). 24
Figure 12: LAIeff, LAI, FAPAR and FCOVER measurements acquired in Maragua_Upper Tana site, during the field campaign 8th March 2016. 25
Figure 13: Distribution of the measured biophysical variables over the ESUs, Maragua_Upper Tana site. Field campaign on 8th March, 2016. 26
Figure 14: Comparison of NDVI distribution between ESUs and over the whole image. Field campaign (8th March, 2016), Maragua_Upper Tana (Kenya). 27
Figure 15: Convex Hull test over 20x20 km^2 (left side) and 5x5 km^2 (right side) areas: clear and dark blue correspond to the pixels belonging to the 'strict' and 'large' convex hulls. Red corresponds to the pixels for which the transfer function is extrapolating, Maragua_Upper Tana, 2016. 29
Figure 16: Test of multiple regression (TF) applied on different band combinations. Band combinations are given in abscissa (1=G, 2=RED, 3=NIR and 4=SWIR). The weighted root mean square error (RMSE) is presented in red along with the cross-validation RMSE in green. The numbers indicate the number of data used for the robust regression with a weight lower than 0.7 that could be considered as outliers. Maragua_Upper Tana, field campaign on 8th March 2016. 31
Figure 17: LAIeff, LAI, FAPAR and FCOVER results for regression on NDVI. Full dots: Weight>0.7. Empty dots: 0<Weight<0.7. Crosses: Weight=0. Maragua_Upper Tana site, field campaign 2016 on 8-9th March, 2016. 33
Figure 18: Ground-based maps 20x20 km^2 retrieved on Maragua_Upper Tana site (Kenya) field campaign (8th March 2016). Left: LAieff Right: LAI. 34
Figure 19: Ground-based of maps (20x20 km^2) retrieved on Maragua_Upper Tana site (Kenya) 2016. Left: FAPAR (8th July). Right: FCOVER. 34

Figure 20: Ground-based of maps (5x5 km^2) retrieved on Maragua_Upper Tana site (Kenya) 2016. ..... *35*
Figure 21: Scatter plots to LAI vs FAPAR and FAPAR vs FCOVER 20x20 km biophysical maps for the field campaign over Maragua_Upper Tana site (Kenya) 8th March, 2016. ..... *36*

LIST OF TABLES

Table 1: Coordinates and altitude of the Maragua site (centre). 15
Table 2: The Header used to describe ESUs with the ground measurements. 24
Table 3: Percentages of Convex hull results over the study area 5x5 km^2 in Maragua_Upper Tana, 2016. Convex hull values: 0= extrapolation of TF, 1= strict convex hull and 2= large convex hull. 28
Table 4: Acquisition geometry of Landsat-8 data used for retrieving high resolution maps. 30
Table 5: Transfer function applied to the whole site for LAIeff, LAI, instantaneous FAPAR at 10:00 SLT and FCOVER. RW for weighted RMSE, and RC for cross-validation RMSE. NDVI$_\infty$ corresponds to NDVI value for fully developed canopies, and NDVI$_S$ to NDVI value for bare soil areas. 32
Table 6: Mean values and standard deviation (STD) of the HR biophysical maps for the selected 3 x 3 km2 areas at Maragua_Upper Tana site (Kenya) 2016. 36
Table 7: Content of the dataset. 37

LIST OF ACRONYMS

CEOS	Committee on Earth Observation Satellite
CEOS LPV	Land Product Validation Subgroup
CIAT	International Center for Tropical Agriculture
DG AGRI	Directorate General for Agriculture and Rural Development
DG RELEX	Directorate General for External Relations (European Commission)
DHP	Digital Hemispheric Photographs
ECV	Essential Climate Variables
EUROSTATS	Directorate General of the European Commission
ESU	Elementary Sampling Unit
FAPAR	Fraction of Absorbed Photo-synthetically Active Radiation
FAO	Food and Agriculture Organization
FCOVER	Fraction of Vegetation Cover
GCOS	Global Climate Observing System
GEO-GLAM	Global Agricultural Geo- Monitoring Initiative
GIO-GL	GMES Initial Operations - Global Land (GMES)
GCOS	Global Climate Observing System
GMES	Global Monitoring for Environment and Security
GPS	Global Positioning System
IMAGINES	Implementing Multi-scale Agricultural Indicators Exploiting Sentinels
JECAM	Joint Experiment for Crop Assessment and Monitoring
LAI	Leaf Area Index
LDAS	Land Data Assimilation System
LUT	Look-up-table techniques
PAI	Plant Area Index
PROBA-V	Project for On-Board Autonomy satellite, the V standing for vegetation.
RMSE	Root Mean Square Error
SPOT /VGT	Satellite Pour l'Observation de la Terre / VEGETATION
SCI	GMES Services Coordinated Interface
SLT	Solar Local Time
TOA	Top of Atmosphere Reflectance
USGS	U.S. Geological Survey Science organization.
UTM	Universal Transverse Mercator coordinates system
VALERI	Validation of Land European Remote sensing Instruments
WGCV	Working Group on Calibration and Validation (CEOS)

1. BACKGROUND OF THE DOCUMENT

1.1. EXECUTIVE SUMMARY

The Copernicus Land Service has been built in the framework of the FP7 geoland2 project, which has set up pre-operational infrastructures. ImagineS intends to ensure the continuity of the innovation and development activities of geoland2 to support the operations of the global land component of the GMES Initial Operation (GIO) phase. In particular, the use of the future Sentinel data in an operational context will be prepared. Moreover, IMAGINES will favor the emergence of new downstream activities dedicated to the monitoring of crop and fodder production.

The main objectives of ImagineS are to (i) improve the retrieval of basic biophysical variables, mainly LAI, FAPAR and the surface albedo, identified as Terrestrial Essential Climate Variables, by merging the information coming from different sensors (PROBA-V and Landsat-8) in view to prepare the use of Sentinel missions data; (ii) develop qualified software able to process multi-sensor data at the global scale on a fully automatic basis; (iii) complement and contribute to the existing or future agricultural services by providing new data streams relying upon an original method to assess the above-ground biomass, based on the assimilation of satellite products in a Land Data Assimilation System (LDAS) in order to monitor the crop/fodder biomass production together with the carbon and water fluxes;(iv) demonstrate the added value of this contribution for a community of users acting at global, European, national, and regional scales.

Further, ImagineS serves the growing needs of international (e.g. FAO and NGOs), European (e.g. DG AGRI, EUROSTATS, DG RELEX), and national users (e.g. national services in agro-meteorology, ministries, group of producers, traders) on accurate and reliable information for the implementation of the EU Common Agricultural Policy, of the food security policy, for early warning systems, and trading issues. ImagineS will also contribute to the Global Agricultural Geo-Monitoring Initiative (GEO-GLAM) by its original agriculture service which can monitor crop and fodder production together with the carbon and water fluxes and can provide drought indicators, and through links with JECAM (Joint Experiment for Crop Assessment and Monitoring).

1.2. PORTFOLIO

The ImagineS portfolio contains global and regional biophysical variables derived from multi-sensor satellite data, at different spatial resolutions, together with agricultural indicators, including the above-ground biomass, the carbon and water fluxes, and drought indices resulting from the assimilation of the biophysical variables in the Land Data Assimilation System (LDAS).

The production in Near Real Time of the 333m resolution products, at a frequency of 10 days, using PROBA-V data is carried out in the Copernicus Global Land Service (http://land.copernicus.eu/global/).

The demonstration of high resolution (30m) products derived from Landsat-8 was done over demonstration sites of cropland and grassland in contrasting climatic and environmental

conditions. Demonstration products are available on the ImagineS website (http://www.fp7-imagines.eu/pages/services-and-products/landsat-8-biophysical-products.php

1.3. SCOPE AND OBJECTIVES

The main objective of this document is two-fold: First, describe the field campaign and ground data collected at Maragua site (Murang'a country), in the Upper Tana basin, Kenya, and secondly, to describe the processing and up-scaling of the ground data to generate ground-based high resolution maps of the following biophysical variables:

- Leaf Area Index (LAI), defined as half of the total developed area of leaves per unit ground surface area (m^2/m^2). We focused on two different LAI quantities (for green elements):
  - The effective LAI (LAIeff) derived from the description of the gap fraction as a function of the view zenith angle. In addition, effective LAI measures derived at 57.5º are also provided in the ground database.
  - The actual LAI (LAI) estimate corrected from the clumping index.
- Fraction of green vegetation cover (FCover), defined as the proportion of soil covered by vegetation, derived from the gap fraction between 0º and 10º of view zenith angle.
- Fraction of Absorbed Photosynthetically Active Radiation (FAPAR), which is the fraction of the photosynthetically active radiation (PAR) absorbed by a vegetation canopy. We are also focused on green elements. PAR is the solar radiation reaching the canopy in the 0.4–0.7 µm wavelength region. We focused on the instantaneous 'black-sky' FAPAR at 10:00h Solar Local Time (SLT), which is the FAPAR under direct illumination conditions at a given solar position. In addition, two other quantities are provided: daily integrated FAPAR computed as the black-sky FAPAR integrated over the day and the 'white-sky' FAPAR, which is the FAPAR under diffuse illumination conditions.

1.4. CONTENT OF THE DOCUMENT

This document is structured as follows:

- Chapter 2 provides an introduction to the field experiment.
- Chapter 3 provides the location and description of the site.
- Chapter 4 describes the ground measurements, including material and methods, sampling and data processing.
- Chapter 5 provides an evaluation of the sampling.
- Chapter 6 describes the production of high resolution ground-based maps, and the selected "mean" values for validation.

2. INTRODUCTION

Validation of remote sensing products is mandatory to guaranty that the satellite products meets the user's requirements. Protocols for validation of global LAIeff products are already developed in the context of Land Product Validation (LPV) group of the Committee on Earth Observation Satellite (CEOS) for the validation of satellite-derived land products (Fernandes et al., 2014), and recently applied to Copernicus global land products based on SPOT/VGT observations (Camacho et al., 2013). This generic approach is made of 2 major components:

- The indirect validation: including inter-comparison between products as well as evaluation of their temporal and spatial consistency
- The direct validation: comparing satellite products to ground measurements of the corresponding biophysical variables. In the case of low and medium resolution sensors, the main difficulty relies on scaling local ground measurements to the extent corresponding to pixels size. However, the direct validation is limited by the small number of sites, for that reason a main objective of ImagineS is the collection of ground truth data in demonstration sites.

The content of this document is compliant with existing validation guidelines (for direct validation) as proposed by the CEOS LPV group (Morisette et al., 2006); the VALERI project (http://w3.avignon.inra.fr/valeri/) and ESA campaigns (Baret and Fernandes, 2012). It therefore follows the general strategy based on a bottom up approach: it starts from the scale of the individual measurements that are aggregated over an elementary sampling unit (ESU) corresponding to a support area consistent with that of the high resolution imagery used for the up-scaling of ground data. Several ESUs are sampled over the site. Radiometric values over a decametric image are also extracted over the ESUs. This will be later used to develop empirical transfer functions for up-scaling the ESU ground measurements (e.g. Martínez et al., 2009). Finally, the high resolution ground based map will be compared with the medium resolution satellite product at the spatial support of the product.

In the framework of ImagineS project, an intensive field campaign conducted by EOLAB and CIAT (International Center for Tropical Agriculture) was carried out on 8th – 9th March for the characterization of vegetation variables in the Maragua site, Kenya.

This report describes the field activities:

- **Field campaign:** 8th – 9th of March, 2016.
- **Teams involved in field collection** (Figure 1):
  CIAT: Justine Cordingley, Kennedy W. Nganga, Jannen Gicheha
  EOLAB: Fernando Camacho

Figure 1: Team involved in the field campaign in Maragua Upper Tana site, Kenya (2016), along with local farmers (those wearing white dressing on the head) in front of a Tee plantation

Contact:

EOLAB: Fernando Camacho (fernando.camacho@eolab.es)

CIAT: Justine Cordingley (j.cordingley@cgiar.org)

3. STUDY AREA

3.1. LOCATION

The study area is located near Maragua city, in the Murang'a country. This site is located in the upper Tana basin, in Kenya (Figure 2). The Maragua site is located at 1600 m elevation, 0.77º South and 36.97º East (Table 1).

Location Study area from GoogleEarth – Landsat8 TOA

Figure 2: Location of Maragua_Upper Tana site in Kenya. False color composition (RGB – SWIR-NIR-RED) of TOA Reflectance Landsat-8 images over the study area 20 km^2. (Maragua Upper Tana, 8th March, 2016).

Table 1: Coordinates and altitude of the Maragua site (centre).

CAMPAIGN	Altitude	Latitud	Longitude
Maragua Upper Tana Geographic Lat/Lon, WGS 84 (degrees)	1600m	0.77º S	+36.97º E

Figure 2-right shows the false composition SWIR-NIR-Red (RGB) over a 20x20 km^2 Top Of Canopy (TOA) Reflectance Landsat-8 images used for up-scaling the ground dataset.

3.2. DESCRIPTION OF THE TEST SITE

The test site is located in the upper Tana river basin. The Tana River has a length of some 1000 km, rising in the Aberdare and Mount Kenya ranges of central Kenya and running through the arid and semi-arid lands in the eastern part of the country to enter the Indian Ocean through a fan-shaped Delta which covers approximately 1.300 km^2. The Tana's catchment covers an area in excess of 100.000 km^2, and contains more than 4 million

people. The Tana River is the only permanent river in this extremely dry region, and constitutes a vital water resource for all sectors of the human population.

Figure 3 shows landscape pictures of the upper Tana River taken during the field campaign. Land use types over the area include tea, coffee, eucalyptus, banana, among others. Figure 4 shows pictures of the typical crops sampled in the area. Note that the area is characterized by quite small plots and a significant spatial (both inter-field and intra-field) heterogeneity.

Figure 3: Landscape views of Maragua site, Kenya, 8th March 2016.

Figure 4: Pictures taken during the field campaign (8th March 2016) in Maragua_Upper Tana site (Kenya) over typical fields.

4. GROUND MEASUREMENTS

The ground measurement database reported here was acquired by EOLAB.

4.1. MATERIAL AND METHODS

A hemispherical digital photography (DHP) camera was used for estimating biophysical variables in the study area.

4.1.1 Digital Hemispheric Photographs (DHP)

DHP were acquired with a digital camera. Hemispherical photos allow the calculation of LAI, FAPAR and FCOVER measuring gap fraction through an extreme wide-angle camera lens (i.e. 180º) (Weiss et al., 2004). It produces circular images that record the size, shape, and location of gaps, either looking upward from within a canopy or looking downward from above the canopy. The used system is composed by a professional camera and a fisheye lens: CANON EOS 6D and a SIGMA 8mm F3.5 – EX DG.

Since optical systems are not perfect, it is needed to calibrate the system in order to determinate the Optical Centre and the Projection Function (Weiss, 2010). The optical centre is defined by the projection of the optical axis onto the CCD matrix where the image is recorded, for the CANON EOS 6D dual system (camera and lens) was found in the point: (x=1378, y=896) (Latorre et al. 2014).

The hemispherical photos acquired during the field campaign were processed with the CAN-EYE software version 6.4 (developed by INRA http://www6.paca.inra.fr/can-eye) to derive LAI, FAPAR and FCOVER. It is based on a RGB colour classification of the image to discriminate vegetation elements from background (i.e., gaps). This approach allows exploiting downward-looking photographs for short canopies (background = soil) as well as upward-looking photographs for tall canopies (background = sky). CAN-EYE software processes simultaneously up to of 20 images acquired over the same ESU. Note that our images were acquired with similar illumination conditions to limit the variation of colour dynamics between images.

The processing is achieved in 3 main steps (Weiss et al., 2004). First, image pre-processing is performed, which includes removing undesired objects (e.g. operator, sun glint) and image contrast adjustments to ensure a better visual discrimination between vegetation elements and background. Second, an automatic classification (k-means clustering) is applied to reduce the total number of distinctive colours of the image to 324 which is sufficient to ensure accurate discrimination capacities while keeping a small enough number of colours to be easily manipulated. Finally, a default classification based on predefined colour segmentation is first proposed and then iteratively refined by the user. The allocation of the colours to each class (vegetation elements versus background) is the most critical phase that needs to be interactive because colours depend both on illumination conditions

and on canopy elements. At the end of this process a binary image, background versus vegetation elements (including both green and non-green elements) is obtained.

The CAN-EYE software computes biophysical variables from gap fraction as follows:

Effective LAI (LAIeff): Among the several methods described in Weiss et al (2004), the effective LAI estimation in the CAN-EYE software is performed by model inversion. The effective LAI is estimated from the Plant Area Index (PAI) which is the variable estimated by CAN-EYE, as no distinction between leaves or other plant elements are made from the gap fraction estimates. PAI is very close to the effective LAI for croplands when pictures are taken downward looking, whereas larger discrepancies are expected for forest when pictures are taken upward looking. Effective LAI is directly retrieved by inverting Eq. (1) (Poisson model) and assuming an ellipsoidal distribution of the leaf inclination using look-up-table (LUT) techniques.

$$P_0(\theta_v, \varphi_v) = e^{-N\cdot(\theta_v,\varphi_v)} = e^{-G\cdot(\theta_v,\varphi_v)\cdot\frac{LAI_{eff}}{\cos(\theta_v)}} \quad \text{Eq. (1)}$$

A large range of random combinations of LAI (between 0 and 10, step of 0.01) and ALA (Average Leaf Angle) (10º and 80º, step of 2º) values is used to build a database made of the corresponding gap fraction values (Eq.1) in the zenithal directions defined by the CAN-EYE user (60º for the DHP collection in this field campaign). The process consists then in selecting the LUT element in the database that is the closest to the measured P_0. The distance (cost function C_k) of the k^{th} element of the LUT to the measured gap fraction is computed as the sum of two terms. The first term computes a weighted relative root mean square error between the measured gap fraction and the LUT one. The second term is the regularization term that imposes constraints to improve the PAI estimates. Two equations are proposed for the second “regularization” term:

(1) constraint used in CAN-EYE V5.1 on the retrieved ALA values that assume an average leaf angle close to 60º ± 03º, and

(2) constraint used in CAN-EYE V6.1 on the retrieved PAI value that must be close from the one retrieved from the zenithal ring at 57º. This constraint is more efficient, but it can be computed only when the 57º ring is available (i.e., COI≥60º)

The software also proposed other ways of computing PAI and ALA effective using Miller’s formula (Miller, 1967) which assumed that gap fraction only depends from view zenith angle. Furthermore, the CAN-EYE makes an estimation using the Welles and Norman (1991) method used in LAI-2000 for 5 rings. These LAI2000-like estimates were not used here as are based on the same Miller’s formula but using limited angular sampling.

LAI: The actual LAI that can be measured only with a planimeter with however possible allometric relationships to reduce the sampling, is related to the effective leaf area index through:

$$LAI_{eff} = \lambda_0 \cdot LAI$$ Eq. (2)

where λ_0 is the clumping index. In CAN-EYE, the clumping index is computed using the Lang and Xiang (1986) logarithm gap fraction averaging method, although some uncertainties are associated to this method (Demarez et al., 2008). The principle is based on the assumption that vegetation elements are locally assumed randomly distributed. Values of clumping index given by CAN_EYE are in certain cases correlated with the size of the cells used to divide photographs.

As the CAN-EYE software provides different results (CEV6.1, CEV5.1 and Miller's) for LAIeff and LAI variables; an average LAI value was provided as ground estimate, and the standard deviation of the different method LAI estimates was reported as the uncertainty of the estimate (see associated ***2016_VGM_Maragua_Upper_Tana.xls*** *file). Note that for LAI, only CEV6.1 and CEV5.1 were used.*

FCOVER is retrieved from gap fraction between 0 to 10°.

$$FCOVER = 1 - P_0 \cdot (0 - 10°)$$ Eq. (3)

FAPAR**:** As there is little scattering by leaves in that particular spectral domain due to the strong absorbing features of the photosynthetic pigments, FAPAR is often assumed to be equal to FIPAR (Fraction of Intercepted Photosynthetically Active Radiation), and therefore directly related to the gap fraction. The actual FAPAR is the sum of two terms, weighted by the diffuse fraction in the PAR domain: the 'black sky' FAPAR that corresponds to the direct component and the 'white sky' or the diffuse component.

The instantaneous "Black-sky FAPAR" ($FPAR^{BS}$) is given at a solar position (date, hour and latitude). Depending on latitude, the CAN EYE software computes the solar zenith angle every solar hour during half the day (there is symmetry at 12:00). The instantaneous FAPAR is then approximated at each solar hour as 1 minus the gap fraction in the corresponding solar zenith angle:

$$FAPAR^{BS}(\theta_S) = 1 - P_0 \cdot (\theta_S)$$ Eq. (4)

The "daily integrated" black-sky FAPAR is computed as the following:

$$FAPAR^{BS}_{Day} = \frac{\int_{sunset}^{sunrise} cos(\theta_S) \cdot [1 - P_0 \cdot (\theta_S)] \cdot d\theta}{\int_{sunset}^{sunrise} cos(\theta_S) \cdot d\theta}$$ Eq. (5)

The "white-sky (or diffuse) FAPAR" is computed as the following:

$$FAPAR^{WS} = \frac{1}{\pi} \int_0^{2 \cdot \pi} \int_0^{\frac{\pi}{2}} P_0 cos(\theta_S) sin(\theta_S) d\theta d\varphi = 2 \cdot \int_0^{\frac{\pi}{2}} P_0 cos(\theta_S) sin(\theta_S) d\theta$$ Eq. (6)

The CAN-EYE software provides the three FAPAR variables. Instantaneous black-sky FAPAR values at 10:00h SLT were up-scaled. No uncertainty estimate in CAN-EYE is provided for FAPAR.

4.2. SPATIAL SAMPLING SCHEME

The spatial sampling scheme follows the recommendation for running a field campaign provided in ImagineS to local teams (Camacho et al., 2015). The fields were selected to sample the range of vegetation types and conditions encountered in the test site, considering accessibility as well. The location of each Elementary Sampling Unit (ESU) was recorded using a GPS that provides an accuracy of few meters. A pseudo-regular sampling was used within each ESU of approximately 20x20 m^2 size. A total of 26 ESUs were characterized (Figure 5). The number of hemispherical photos per ESU ranges between 12 and 15.

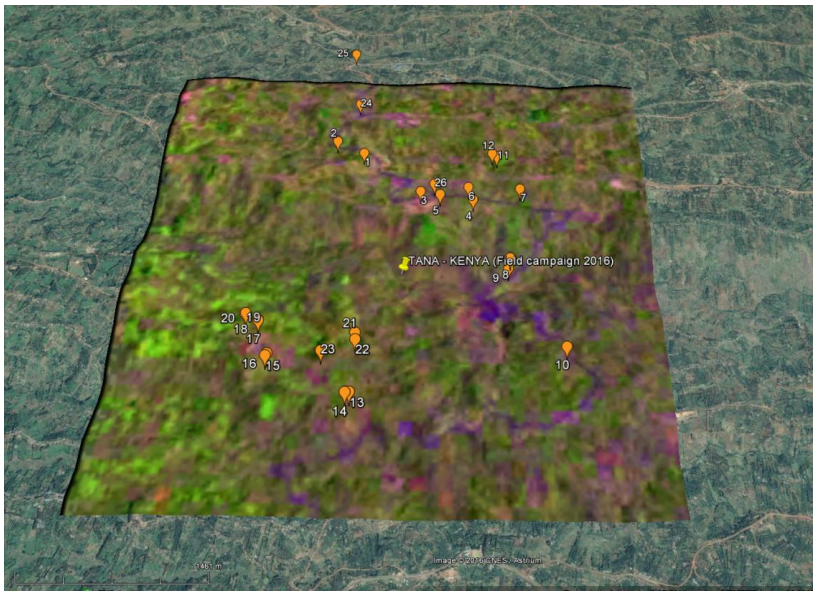

Figure 5: Location of the Elementary Sampling Units (ESU) over the study area in *Maragua_Upper Tana* site. Field campaign (8th-9th March 2016). DHP sampling over Google Earth and TOA Landsat-8 footprint.

Additional elementary sampling units (ESU) over Bare Soils were selected to complete the representation of the variability in the study area.

4.3. GROUND DATA

4.3.1. Data processing

The software CAN-EYE version V6.4 was used to process the DHP images. Figure 6 shows some examples of DHP over several ESUs.

Figure 6: Digital Hemispherical Photographs acquired in *Maragua_Upper Tana* site (Kenya) during the field campaign on 8-9th March, 2016. Top: Upward Looking. Bottom: Downward Looking.

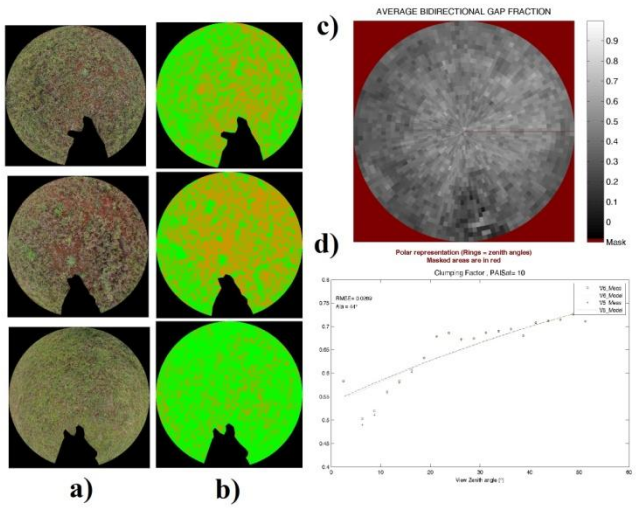

Figure 7: Results of the CAN-EYE processing carried out on ESU 23 (grassland) during the field campaign (8-9th March, 2016). (a) DHP images. (b) Classified images. (c) Average bidirectional gap fraction and (d) the clumping factor versus view zenith angle.

Figure 7 shows an example of the CAN-EYE processing results carried out on ESU 23 (grassland) during the field campaign. Different results of the CAN-EYE processing are shown: (a) the DHP over the ESU, (b) the classified vegetation/soil image generated by the software, (c) the average bidirectional gap fraction and (d) the clumping factor as a function of the view zenith angle.

As described in section 4.1, CAN-EYE provides the LAI and effective LAI values by using three different methods: CEV6.1, CEV5.1 and Miller's. Figure 8 shows the inter-comparison between the three methods. For LAIeff, the results are very similar and the average of the three estimations is provided on the ground dataset. However, for the LAI, the scattering between methods is much higher for medium values, displaying Miller's method lowest estimations than CEV6.1 and CEV5.1. It can be explained because the Miller's method does not consider all the viewing angles. Consequently, this method has been discarded for the LAI average in the ground dataset.

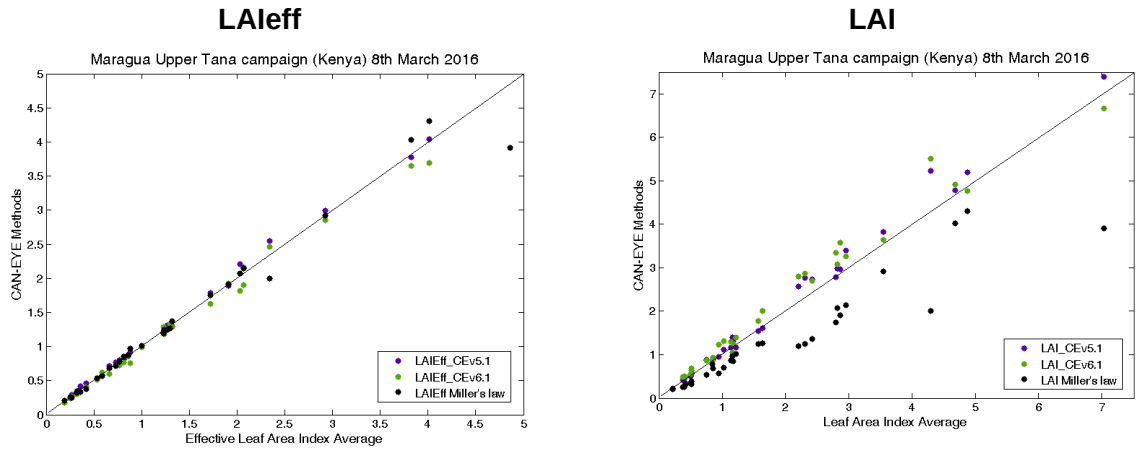

Figure 8: Inter-comparison of the calculated biophysical variables LAIeff (left side) and LAI (right side) over the ESUs with different methods: CEV5.1, CEV6.1 and Miller´s formula. Maragua_Upper Tana site (Kenya) during the campaign of 8-9th March, 2016.

4.3.1.1. Special cases: ESUs with understory and overstory

For several ESUs (1, 7, 10 - 14) with understory and overstory, hemispherical images were acquired upward looking for characterizing the overstory and downward looking for the understory (Figure 9). The two sets of acquisitions were processed separately to derived LAI (effective and true), FCOVER and FAPAR. To compute FCOVER and FAPAR, the independency of the gaps inside the understory and the gaps inside the trees has been assumed. The ESU biophysical variables were then computed as:

- LAI :

$$LAI = LAI_{ABOVE} + LAI_{BELOW}$$

- FCOVER / FAPAR :

$$FCOVER = 1 - (1 - FCOVER_{ABOVE})(1 - FCOVER_{BELOW})$$

$$FAPAR = 1 - (1 - FAPAR_{ABOVE})(1 - FAPAR_{BELOW})$$

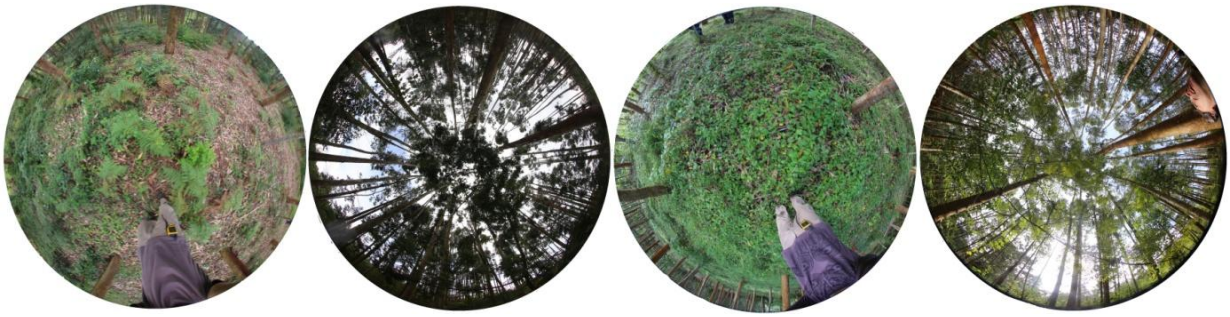

Figure 9: Examples of understory and overstory over Eucalyptus plantation: ESU 7 (left side) and ESU 11(right side).

Figure 10 shows the inter-comparison between LAI with instantaneous FAPAR at 10:00 SLT. The typical positive exponential curve is observed. Both variables (LAI and LAIeff) are presented at the same graph where similar exponential trends are observed.

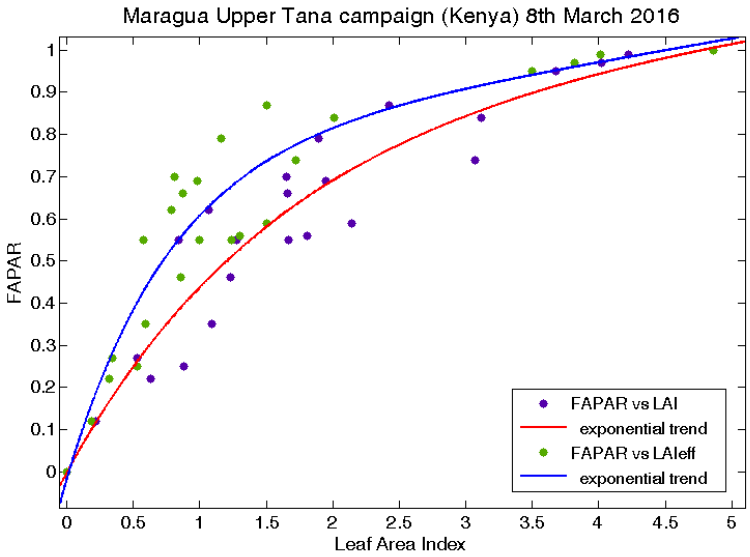

Figure 10: Inter-comparison of the measured biophysical variables over the ESUs. LAI versus FAPAR, Maragua_Upper Tana site (Kenya). Field campaign (8-9th March). LAI (purple dots) and LAIeff (green dots).

Figure 11 shows the inter-comparison between FAPAR and FCOVER, the typical linear relationship is observed. Note that very similar retrievals are observed, slightly higher for FAPAR.

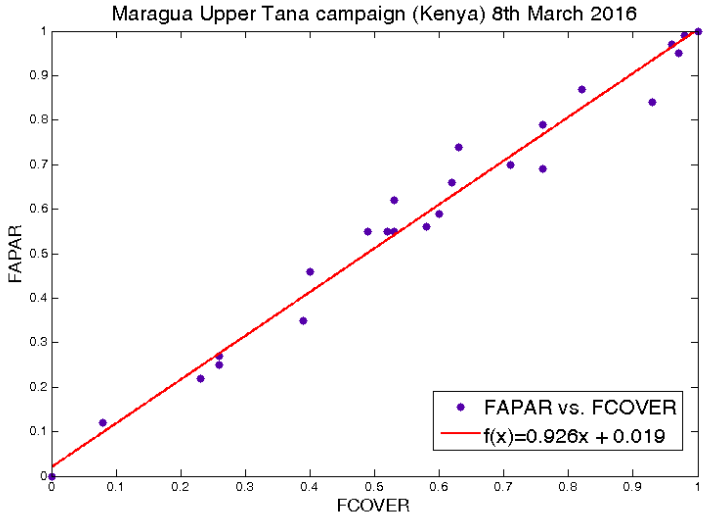

Figure 11: Inter-comparison of the measured biophysical variables over the ESUs. FAPAR versus FCOVER, Maragua Upper Tana site (Kenya). Field campaign (8th March, 2016).

4.3.2. Content of the Ground Dataset

Each ESU is described according to a standard format. The header of the database is shown in Table 2.

Table 2: The Header used to describe ESUs with the ground measurements.

Column	Var.Name		Comment
1	Plot #		Number of the field plot in the site
2	Plot Label		Label of the plot in the site
3	ESU #		Number of the Elementary Sampling Unit (ESU)
4	ESU Label		Label of the ESU in the campaign
5	Northing Coord.		Geographical coordinate: Latitude (º), WGS-84
6	Easting Coord.		Geographical coordinate: Longitude (º), WGS-84
7	Extent (m) of ESU (diameter)		Size of the ESU (1)
8	Land Cover		Detailed land cover
9	Start Date (dd/mm/yyyy)		Starting date of measurements
10	End Date (dd/mm/yyyy)		Ending date of measurements
11	Products*	Method	Instrument
12		Nb. Replications	Number of Replications
13		PRODUCT	Methodology
14		Uncertainty	Standard deviation

*LAIeff, LAI, FAPAR and FCOVER

Figure 12 shows the biophysical parameters obtained during the field experiment. Note that for all variables, additional ESU control points were included in order to extend the sampling over bare areas. The LAIeff ranges between 0.19 (ESU 3 - Grass) and 4.86 (ESU 20 - Tea), with similar distributions but larger values for LAI (ranging from 0.2 to 5.2). The FAPAR values varies between 0.12 (ESU 3 – Grass) to maximum values (0.95 to 1) for the densest Tea fields (e.g. ESU 20). Very similar results are obtained for FCOVER.

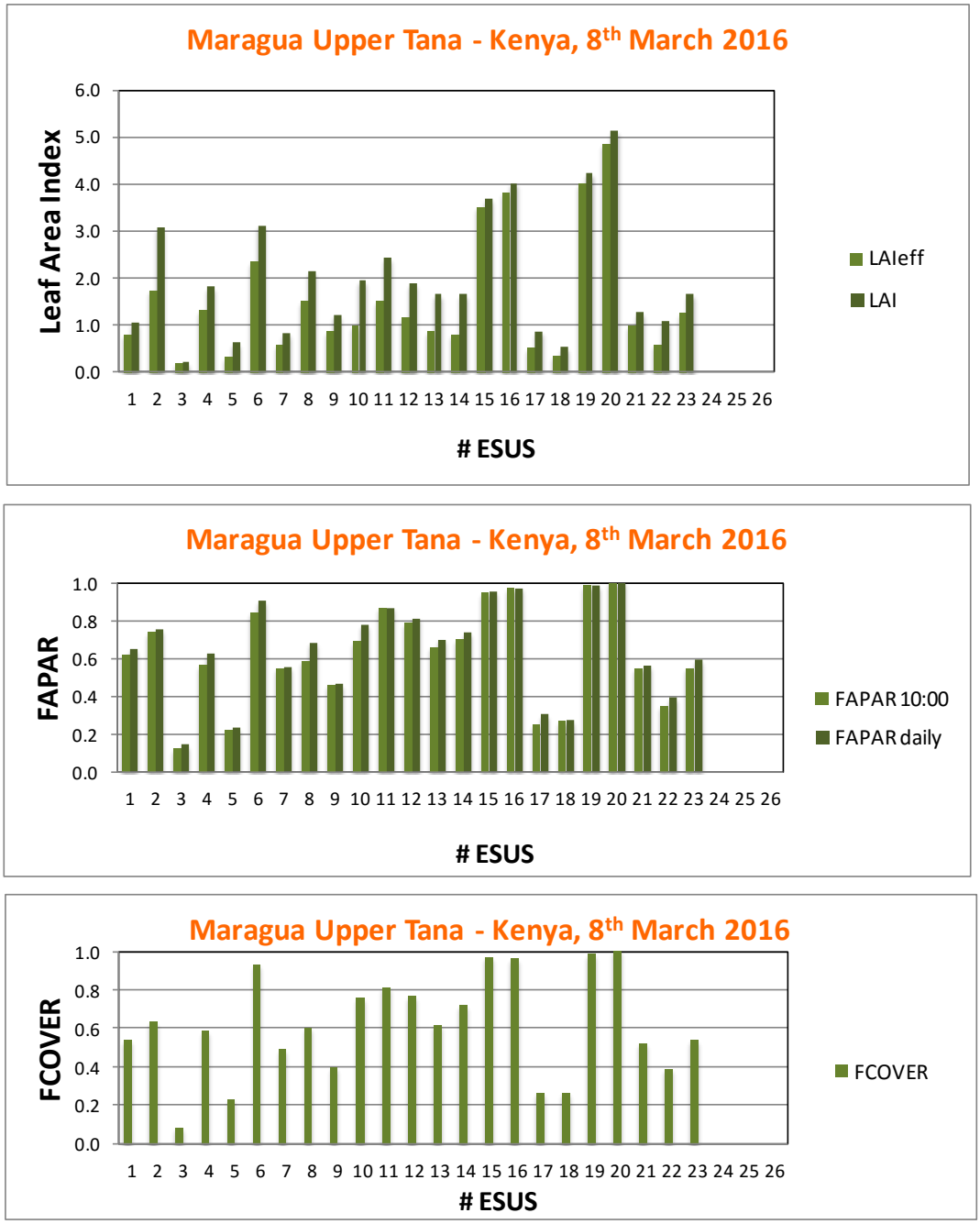

Figure 12: LAIeff, LAI, FAPAR and FCOVER measurements acquired in Maragua_Upper Tana site, during the field campaign 8th March 2016.

Histograms of the measurements are presented in Figure 13. Larger number of cases occurs for medium values (LAI between 2 and 2.5, FAPAR/FCOVER between 0.6 and 0.7).

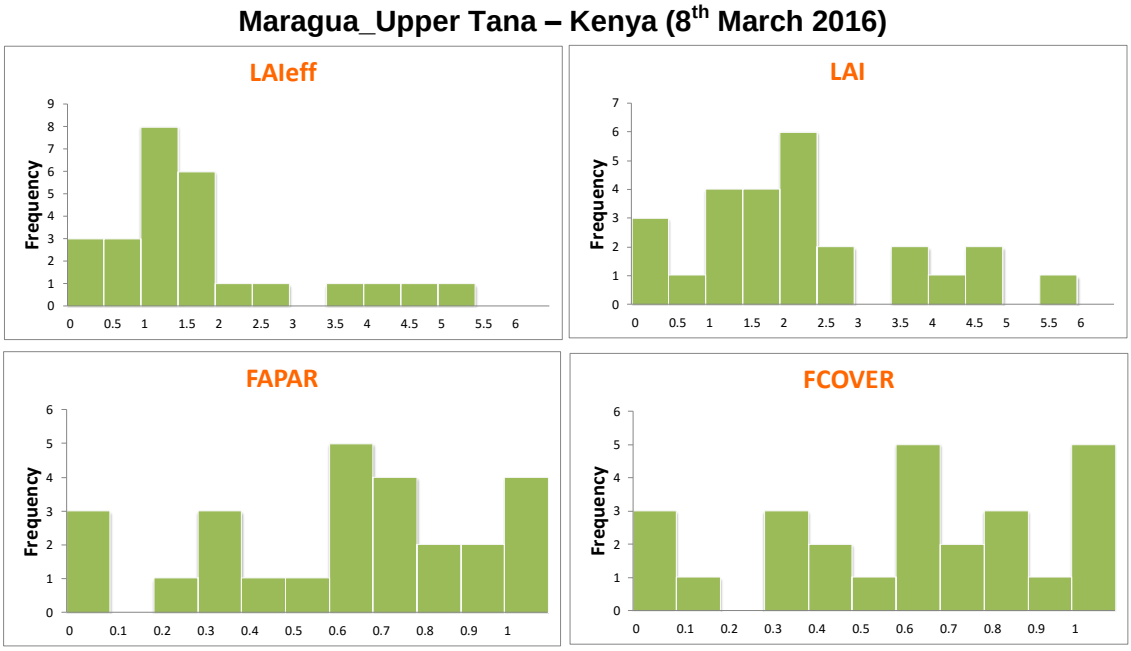

Figure 13: Distribution of the measured biophysical variables over the ESUs, Maragua_Upper Tana site. Field campaign on 8th March, 2016.

5. EVALUATION OF THE SAMPLING

5.1. PRINCIPLES

The data set sampling was concentrated in the areas around the center site. The number of sampling points (included ESUs and ground control points (GCP)) was 26.

5.2. EVALUATION BASED ON NDVI VALUES

The sampling strategy is evaluated using the Landsat-8 image by comparing the NDVI distribution over the site with the NDVI distribution over the ESUs (Figure 14). As the number of pixels is drastically different for the ESU and whole site (WS) it is not statistically consistent to directly compare the two NDVI histograms. Therefore, the proposed technique consists in comparing the NDVI cumulative frequency of the two distributions by a Monte-Carlo procedure which aims at comparing the actual frequency to randomly shifted sampling patterns. It consists in:

1. computing the cumulative frequency of the *N* pixel NDVI that correspond to the exact ESU locations; then, applying a unique random translation to the sampling design (modulo the size of the image)
2. computing the cumulative frequency of NDVI on the randomly shifted sampling design
3. repeating steps 1 and 2, 199 times with 199 different random translation vectors.

This provides a total population of $N = 199 + 1$(actual) cumulative frequency on which a statistical test at acceptance probability $1 - \alpha = 95\%$ is applied: for a given NDVI level, if the actual ESU density function is between two limits defined by the $N\alpha / 2 = 5$ highest and lowest values of the 200 cumulative frequencies, the hypothesis assuming that WS and ESU NDVI distributions are equivalent is accepted, otherwise it is rejected.

Figure 14 shows that the NDVI distribution of Maragua_Upper Tana campaign is slightly biased towards the lower NDVI values

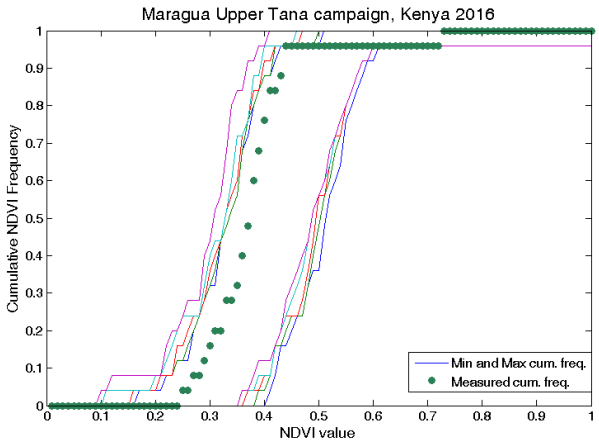

Figure 14: Comparison of NDVI distribution between ESUs and over the whole image. Field campaign (8th March, 2016), Maragua_Upper Tana (Kenya).

5.3. EVALUATION BASED ON CONVEX HULL: PRODUCT QUALITY FLAG.

The interpolation capabilities of the empirical transfer function used for up-scaling the ground data using decametric images is dependent of the sampling (Martinez et al., 2009). A test based on the convex hulls was also carried out to characterize the representativeness of ESUs and the reliability of the empirical transfer function using the different combinations of the selected bands (green, red, NIR and SWIR) of the Landsat-8 image. A flag image is computed over the reflectances. The result on convex-hulls can be interpreted as:

- pixels inside the 'strict convex-hull': a convex-hull is computed using all the Landsat-8 reflectances corresponding to the ESUs belonging to the class. These pixels are well represented by the ground sampling and therefore, when applying a transfer function the degree of confidence in the results will be quite high, since the transfer function will be used as an interpolator;

- pixels inside the 'large convex-hull': a convex-hull is computed using all the reflectance combinations (±5% in relative value) corresponding to the ESUs. For these pixels, the degree of confidence in the obtained results will be quite good, since the transfer function is used as an extrapolator (but not far from interpolator);

- pixels outside the two convex-hulls: this means that for these pixels, the transfer function will behave as an extrapolator which makes the results less reliable. However, having a priori information on the site may help to evaluate the extrapolation capacities of the transfer function.

Figure 15 shows the results of the Convex-Hull test (i.e., Quality Flag image) for the Maragua_Upper Tana site over a 20x20 km^2 and 5x5 km^2 areas around the central coordinate site. The strict and large convex-hulls are high around the test site, 92% and 98% over these areas respectively (Table 3).

Table 3: Percentages of Convex hull results over the study area in Maragua_Upper Tana, 2016. Convex hull values: 0= extrapolation of TF, 1= strict convex hull and 2= large convex hull.

Field Campaign	Quality Flags (%)					
SITE	5x5 km^2			20x20 km^2		
	0	1	2	0	1	2
Maragua Upper Tana	2	97	1	8	90	2

Maragua_Upper Tana (Kenya) – 8th March 2016

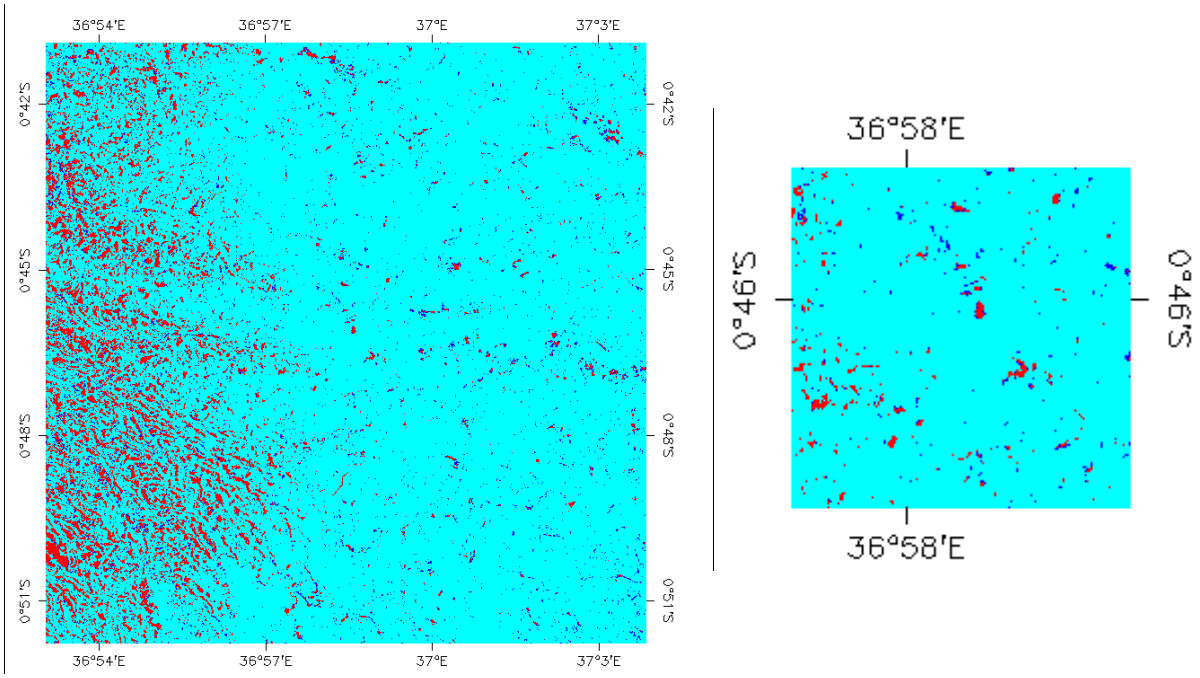

Figure 15: Convex Hull test over 20x20 km^2 (left side) and 5x5 km^2 (right side) areas: clear and dark blue correspond to the pixels belonging to the 'strict' and 'large' convex hulls. Red corresponds to the pixels for which the transfer function is extrapolating, Maragua_Upper Tana, 2016.

6. PRODUCTION OF GROUND-BASED MAPS

6.1. IMAGERY

The Landsat-8 image was acquired the 25th February, 2016 (Table 4 for acquisition geometry). We selected 4 spectral bands from 500 nm to 1750 nm with a nadir ground sampling distance of 30 m. For the transfer function analysis, the input satellite data used is Top of Atmosphere (TOA) reflectance. The original projection is UTM 33 North, WGS-84.

Table 4: Acquisition geometry of Landsat-8 data used for retrieving high resolution maps.

Landsat-8 METADATA	
Platform / Instrument	Landsat-8 / OLI_TIRS
Path	168
Row	60
Selected Bands	B3(green) : 0.53-0.59 µm B4(red) : 0.64-0.67 µm B5(NIR) : 0.85-0.88 µm B6(SWIR1) : 1.58-1.65 µm
	Maragua Upper Tana - Kenya **8th March, 2016**
Acquisition date	2016.02.25 12:34:36
Illumination Azimuth angle	107.95723º
Illumination Elevation angle	58.53376º
Ground control points verify	158
Geometric RMSE Verify	6.293

6.2. THE TRANSFER FUNCTION

The measurements during the field campaign were collected a week before than the acquisition date of the Landsat-8 image used for the up-scaling due to the low variations over the ground data with the field campaign.

6.2.1. The regression method

If the number of ESUs is enough, multiple robust regression 'REG' between ESUs reflectance and the considered biophysical variable can be applied (Martínez et al., 2009):

we used the 'robustfit' function from the Matlab statistics toolbox. It uses an iteratively re-weighted least squares algorithm, with the weights at each iteration computed by applying the bi-square function to the residuals from the previous iteration. This algorithm provides lower weight to ESUs that do not fit well.

The results are less sensitive to outliers in the data as compared with ordinary least squares regression. At the end of the processing, two errors are computed: weighted RMSE (using the weights attributed to each ESU) (RW) and cross-validation RMSE (leave-one-out method) (RC).

As the method has limited extrapolation capacities, a flag image (Figure 15), based on the convex hulls, is included in the final ground based map in order to inform the users on the reliability of the estimates.

6.2.2. Band combination

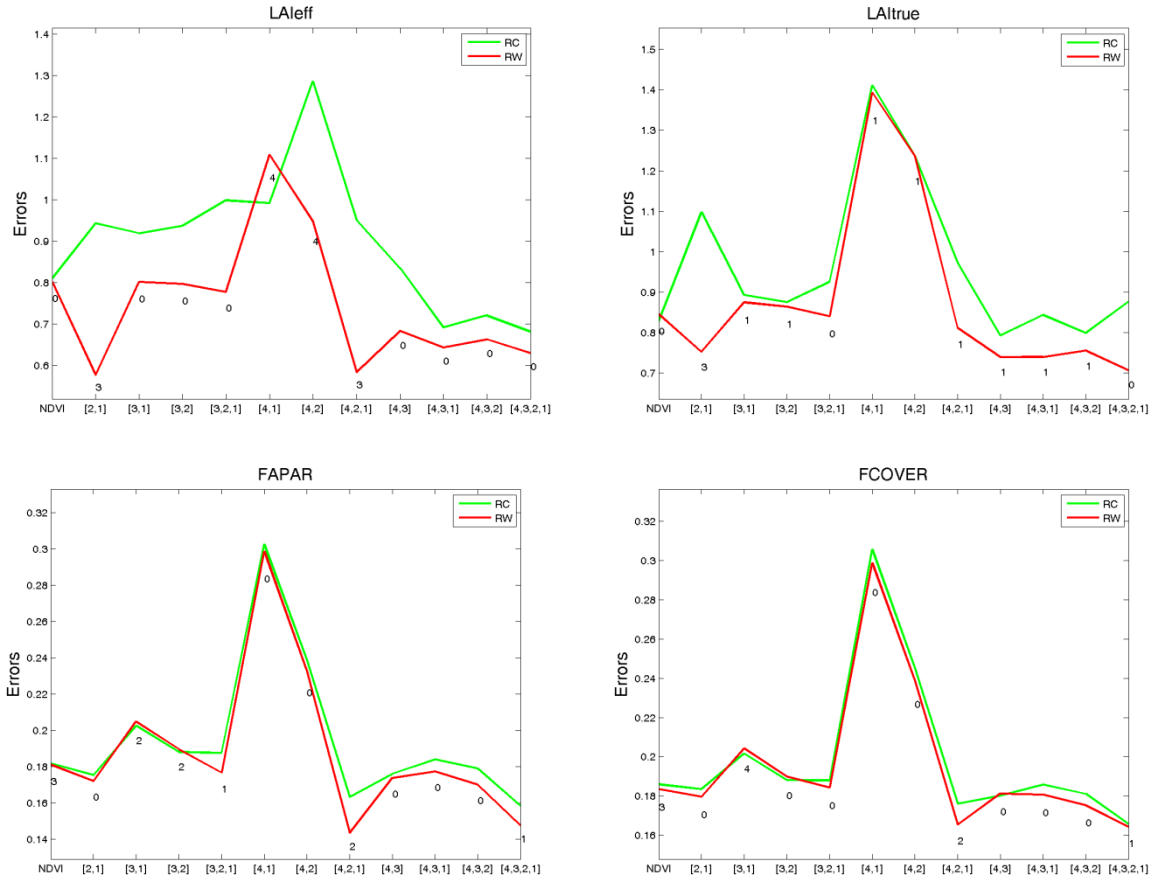

Figure 16: Test of multiple regression (TF) applied on different band combinations. Band combinations are given in abscissa (1=G, 2=RED, 3=NIR and 4=SWIR). The weighted root mean square error (RMSE) is presented in red along with the cross-validation RMSE in green. The numbers indicate the number of data used for the robust regression with a weight lower than 0.7 that could be considered as outliers. Maragua_Upper Tana, field campaign on 8th March 2016.

Figure 16 shows the errors (RW, RC) obtained for the several band combinations using TOA reflectance for field campaign. We have selected the four bands combination as input for the transfer function. It shows, in all cases, lower errors than other combinations, while providing a good consistency of the maps over the whole area (see Figure 21).

6.2.3. The selected Transfer Function

The applied transfer function is detailed in Table 5, along with its weighted (RW) and cross validated (RC) errors.

Table 5: Transfer function applied to the whole site for LAIeff, LAI, instantaneous FAPAR at 10:00 SLT and FCOVER. RW for weighted RMSE, and RC for cross-validation RMSE. $NDVI_\infty$ corresponds to NDVI value for fully developed canopies, and $NDVI_S$ to NDVI value for bare soil areas.

Variable	Band Combination	RW	RC
Maragua Upper Tana campaign, Kenya. 8th March 2016			
LAIeff	-8.71162 -0.00040·(**SWIR**) +0.00039·(**NIR**)-0.00087·(**R**)+0.00179·(**G**)	0.63	0.59
LAI	-6.64002 -0.00040·(**SWIR**) +0.00031·(**NIR**)-0.00132·(**R**)+0.00218·(**G**)	0.71	0.68
FAPAR	-0.71298 -0.00009·(**SWIR**) +0.00003·(**NIR**)-0.00049·(**R**)+0.00069·(**G**)	0.15	0.13
FCOVER	-0.67597 -0.00008·(**SWIR**) +0.00004·(**NIR**)-0.00044·(**R**)+0.00060·(**G**)	0.16	0.15

Figure 17 shows scatter-plots between ground observations and their corresponding transfer function (TF) estimates for the selected bands combination (i.e. the four bands SNRG). A good correlation is observed for the LAIeff, LAI, FAPAR and FCOVER with points distributed along the 1:1 line, with no mean bias and acceptable RMSE values.

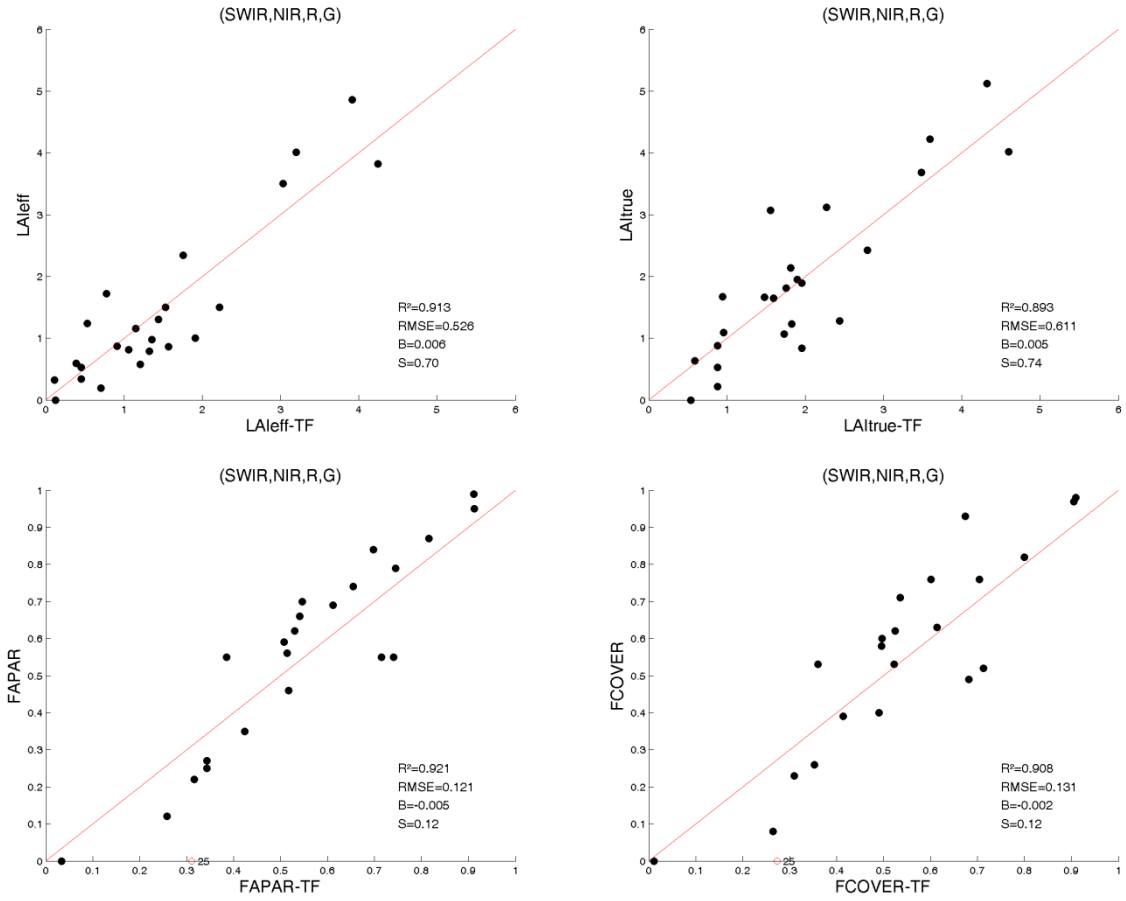

Figure 17: LAIeff, LAI, FAPAR and FCOVER results for regression on (SWIR, NIR, R, G) combination. Full dots: Weight>0.7. Empty dots: 0<Weight<0.7. Crosses: Weight=0. Maragua_Upper Tana site, field campaign 2016 on 8th-9th March, 2016.

6.3. THE HIGH RESOLUTION GROUND BASED MAPS

The high resolution maps are obtained applying the selected transfer functions (Table 5) to the Landsat-8 NDVI derived from TOA reflectances. The study area has been extended to 20x20km^2 (centre located at 0.77 S, 36.97 E, UTM zone 37 South, Datum WGS-84). Figure 18 and Figure 19 present the TF biophysical variables. Figure 15 shows the Quality Flag included in the final product.

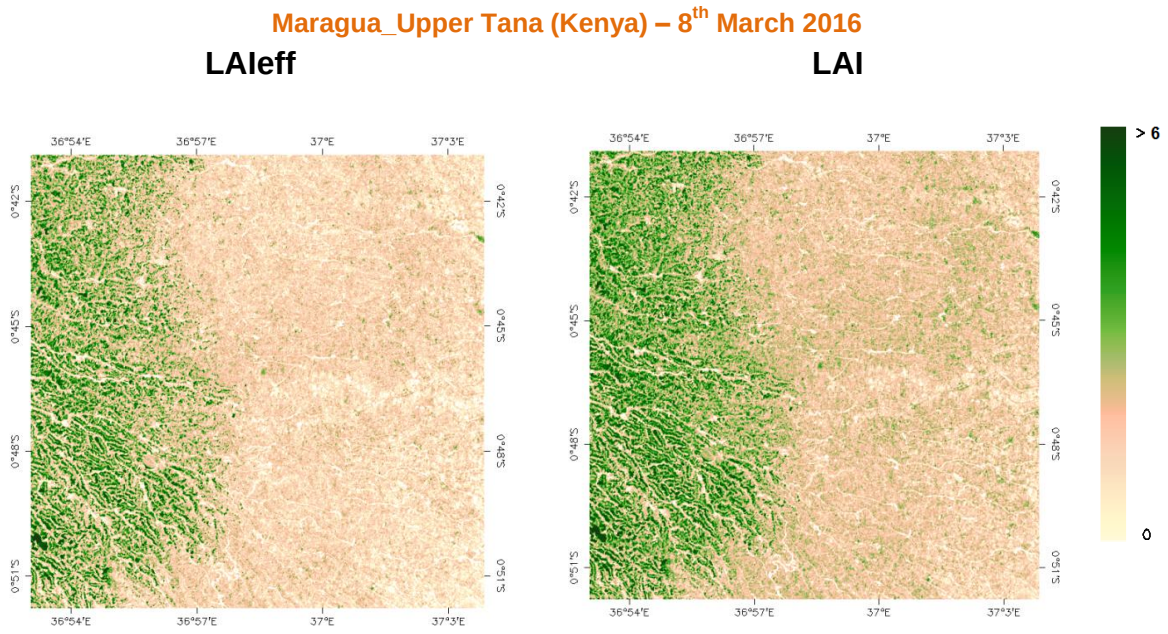

Figure 18: Ground-based maps (20x20 km^2) retrieved on *Maragua_Upper Tana site (Kenya)* field campaign (8th March 2016). Left: LAIeff, Right: LAI.

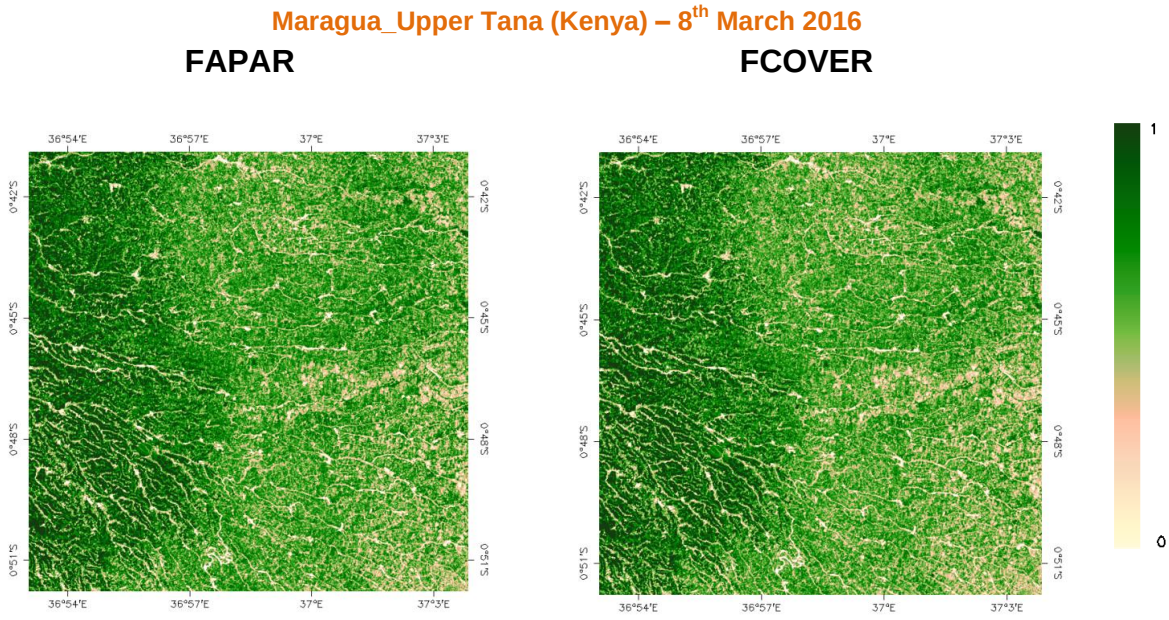

Figure 19: Ground-based of maps (20x20 km^2) retrieved on Maragua_Upper Tana site (Kenya) 2016. Left: FAPAR (8th July). Right: FCOVER.

Figure 20 summarizes these ground-based high resolution maps over the 5x5 km2 study area. These maps are provided for validation of satellite products at coarser resolutions.

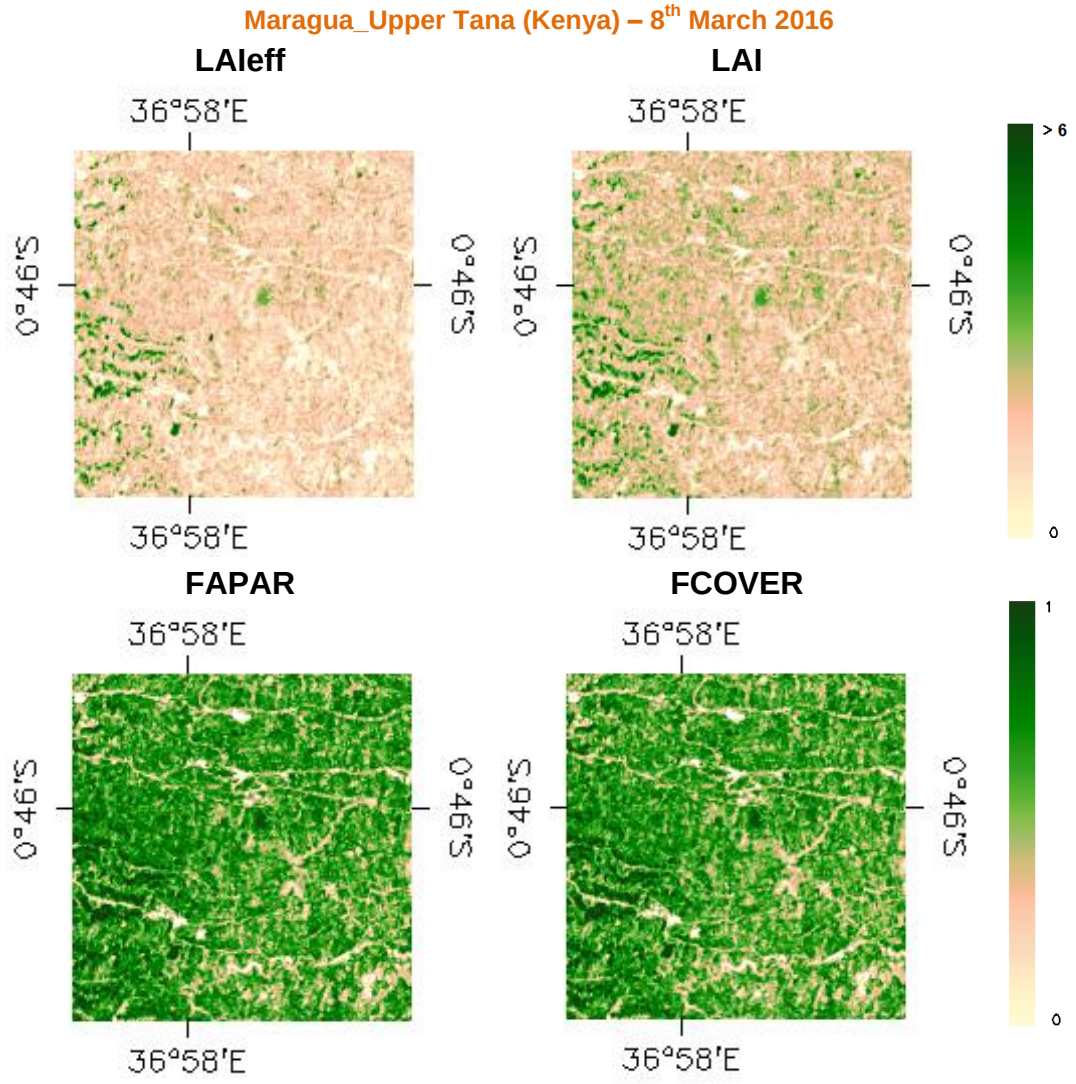

Figure 20: Ground-based of maps (5x5 km^2) retrieved on Maragua_Upper Tana site (Kenya) 2016.

Figure 21 shows several scatters plots between biophysical variables that prove the good consistency of the ground-based maps, showing the exponential (LAI vs FAPAR) and linear (FAPAR vs FCOVER) trend observed with the ground data.

Maragua Upper Tana (Kenya) – 8th March 2016

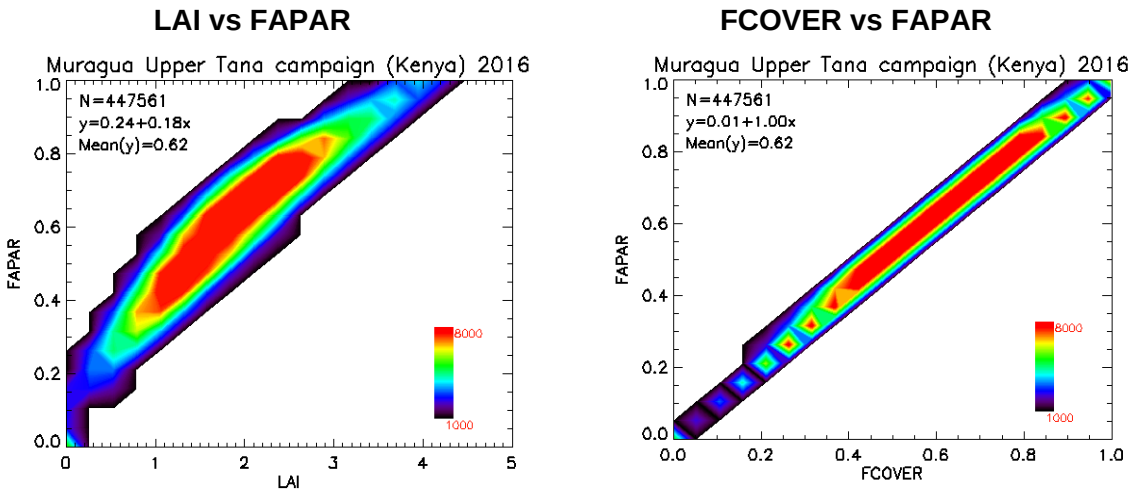

Figure 21: Scatter plots to LAI vs FAPAR and FAPAR vs FCOVER 20x20 km biophysical maps for the field campaign over Maragua_Upper Tana site (Kenya) *8th March, 2016*.

6.3.1. Mean Values

Mean values of a 3x3 km^2 area centred in the test site are provided for the validation of 1 km satellite products in agreement with the CEOS OLIVE DIRECT dataset (Table 6). For the validation of coarser resolutions product (e.g. MSG products) a larger area should be considered.

Table 6*: Mean values and standard deviation (STD) of the HR biophysical maps for the selected 3 x 3 km2 areas at Maragua_Upper Tana site (Kenya) 2016.*

Maragua Upper Tana -Kenya					
LATITUDE	LONGITUDE	LAIeff	LAI	FAPAR	FCOVER
-0.772020° N	+36.97420° E	Mean Values			
3x3 km^2 8th March 2016		1.39	1.88	0.60	0.58
		STDV Values			
		0.67	0.69	0.16	0.16

Table 7 describes the content of the geo-biophysical maps in the "BIO_YYYYMMDD_LANDSAT8_ Maragua Upper Tana_ETF_Area" files.

Nomenclature: BIO_YYYYMMDD_SENSOR_Site_ETF_Area
where:

BIO stands for Biophysical (LAIeff, LAI, FAPAR and FCOVER)

SENSOR = LANDSAT8

YYYYMMDD = Campaign date

Site = Maragua_Upper_Tana

ETF stands for Empirical Transfer Function

Area = window size 20x20 and 5x5

Table 7: Content of the dataset.

Parameter	Dataset name	Range	Variable Type	Scale Factor	No Value
LAI effective	LAIeff	[0, 7]	Integer	1000	-1
LAI	LAI	[0, 7]	Integer	1000	-1
FAPAR 10:00 SLT	FAPAR	[0, 1]	Integer	10000	-1
Fraction of Vegetation Cover	FCOVER	[0, 1]	Integer	10000	-1
Quality Flag	QFlag	0,1,2 (*)	Integer	N/A	-1

(*) 0 means extrapolated value (low confidence), 1 strict interpolator (best confidence), 2 large interpolator (medium confidence).

7. CONCLUSIONS

The FP7 ImagineS project continues the innovation and development activities to support the operations of the Copernicus Global Land service. One of the sites characterized in the framework of the ImagineS project is the Maragua_Upper Tana site, in Kenya.

This report firstly presents the ground data collected during an intensive field campaign on 8th-9th of March, 2016. The dataset includes 26 elementary sampling units where digital hemispherical photographs were taken and processed with the CAN-EYE software version 6.4 to provide LAI, LAIeff, FAPAR and FCOVER values.

Secondly, high resolution ground-based maps of the biophysical variables have been produced over the site. Ground-based maps have been derived using high resolution imagery (Landsat-8 TOA Reflectance) according to the CEOS LPV recommendations for validation of low resolution satellite sensors. Transfer functions have been derived by multiple robust regressions between ESU's reflectance and the several biophysical variables. Four bands combination (R, G, N, SWIR) has been selected for the transfer function, providing lowest errors and good consistency of the maps over the whole area. The RMSE values for the several transfer function estimates are 0.53 for LAIeff, 0.61 for LAI, 0.12 for instantaneous FAPAR at 10:00 SLT and finally 0.13 for FCOVER.

A quality flag map based on the convex-hull is also provided, which shows good confidence of the transfer function (i.e., behaves as interpolator) in 98% at 5x5 km^2 and 92% at 20x20 km^2.

The biophysical variable maps are provided in geographic (UTM 37 South projection WGS-84) coordinates at 30 m resolution. Mean values and standard deviation for LAIeff, LAI, FCOVER and FAPAR were computed over an area of 3x3 km^2 for validation of low and medium resolution satellite products.

8. ACKNOWLEDGEMENTS

This work is supported by the FP7 IMAGINES project under Grant Agreement N°311766. Landsat-8 HR imagery is provided through the USGS Global Visualization service. This work is done in collaboration with the consortium implementing the Global Component of the Copernicus Land Service.

Thanks to CIAT for the support and the organization of the field campaign, and the facilities which allow us to properly characterize the site.

9. REFERENCES

Baret, F., de Solan, B., Lopez-Lozano, R., Ma, K. and Weiss, M. (2010) GAI estimates of row crops from downward looking digital photos taken perpendicular to rows at 57.5º zenith angle: theoretical considerations based on 3D architecture models and application to wheat crops. Agricultural and Forest Metereology. 150, 1393-1401.

Baret, F and Fernandes, R. (2012). Validation Concept. VALSE2-PR-014-INRA, 42 pp.

Berguer. M. M. Rast, P. Wursteisen, E. Attema, J. Moreno, et al. (2001). The DAISEX campaigns in support of a future land-surface-processes mission. Esa bulletin, Bulletin ASE. European Space Agency, nº105: 101-111, February 2001.

Camacho, F., Baret, F., and Lacaze R. (2015). Guidelines for a Field campaign. (Available at ImagineS website: http://fp7-imagines.eu/pages/documents.php).

Camacho, F., Cernicharo, J., Lacaze, R., Baret, F., and Weiss, M. (2013). GEOV1: LAI, FAPAR Essential Climate Variables and FCOVER global time series capitalizing over existing products. Part 2: Validation and intercomparison with reference products. *Remote Sensing of Environment, 137: 310-329.*

Demarez, V., Duthoit, S., Baret, F., Weiss, M. and Dedieu, G. (2008). Estimation of leaf area and clumping indexes of crops with hemispherical photographs. *Agricultural and Forest Meteorology. I48, 644-655*.

Fernandes, R., Plummer, S., Nightingale, J., et al. (2014). Global Leaf Area Index Product Validation Good Practices. CEOS Working Group on Calibration and Validation - Land Product Validation Sub-Group. *Version 2.0: Public version made available on LPV website*.

Latorre, C., Camacho, F., Pérez, M., Beget M.E. and Di Bella, C. (2014). “Vegetation Field Data and Production of Ground-Based Maps: 25 de Mayo site. La Pampa, Argentina” report. 18 -20 (Available at ImagineS website: http://fp7-imagines.eu/pages/documents.php).

Martínez, B., García-Haro, F. J., & Camacho, F. (2009). Derivation of high-resolution leaf area index maps in support of validation activities: Application to the cropland Barrax site. *Agricultural and Forest Meteorology, 149, 130–145*.

Miller, J.B. (1967). A formula for average foliage density. Aust. J. Bot., 15:141-144

Morisette, J. T., Baret, F., Privette, J. L., Myneni, R. B., Nickeson, J. E., Garrigues, S., et al. (2006). Validation of global moderate-resolution LAI products: A framework proposed within the CEOS land product validation subgroup. *IEEE Transactions on Geoscience and Remote Sensing, 44, 1804–1817*.

Weiss, M., Baret, F., Smith, G.J., Jonckheere, I. and Coppin, P., (2004). Review of methods for in situ leaf area index (LAI) determination. Part II. Estimation of LAI, errors and sampling. *Agricultural and Forest Meteorology. 121, 37–53*.

Weiss M. and Baret F. (2010). CAN-EYE V6.1 User Manual

Welles, J.M. and Norman, J.M., 1991. Instrument for indirect measurement of canopy architecture. Agronomy J., 83(5): 818-825.